AIAA 2000–2681

FLOW QUALITY MEASUREMENTS IN THE NASA AMES UPGRADED 11–BY 11–FT TRANSONIC WIND TUNNEL (INVITED PAPER)

M. A. Amaya
NASA Ames Research Center
and
S. V. Murthy
Sverdrup Technology, Inc.

Moffett Field, CA

21st AIAA Aerodynamic Measurement Technology and Ground Testing Conference
19-22 June 2000 / Denver, CO

For permission to copy or to republish, contact the American Institute of Aeronautics and Astronautics, 1801 Alexander Bell Drive, Suite 500, Reston, VA, 20191-4344.

AIAA 2000–2681

FLOW QUALITY MEASUREMENTS IN THE NASA AMES UPGRADED 11–BY 11–FOOT TRANSONIC WIND TUNNEL

by

Max A. Amaya† and Sreedhara V. Murthy§
NASA Ames Research Center Sverdrup Technology Inc.,
Moffett Field, CA 94035

ABSTRACT

Among the many upgrades designed and implemented in the NASA Ames 11-by 11-Foot Transonic Wind Tunnel over the past few years, several directly affect flow quality in the test section: a turbulence reduction system with a honeycomb and two screens, a flow smoothing system in the back leg diffusers, an improved drive motor control system, and a full replacement set of composite blades for the compressor. Prior to the shut–down of the tunnel for construction activities, an 8-foot span rake populated with flow instrumentation was traversed in the test section to fully document the flow quality and establish a baseline against which the upgrades could be characterized. A similar set of measurements was performed during the recent Integrated Systems Test trials, but the scope was somewhat limited in accordance with the primary objective of such tests, namely to return the tunnel to a fully operational status. These measurements clearly revealed substantial improvements in flow angularity and significant reductions in turbulence level for both full–span and semi–span testing configurations, thus making the flow quality of the tunnel one of the best among existing transonic facilities.

† Aero Engineer, Wind Tunnel Operations Branch

§ Sr Engineer, NASA Ames Aero Testing, Ops & Maint. Div.

Copyright © 2000 by the American Institute of Aeronautics and Astronautics, Inc. No copyright is asserted in the United States under Title 17, U.S. Code. The U.S. Government has a royalty–free license to exercise all rights under the copyright claimed herein for Governmental purposes. All other rights are reserved by the copyright owner.

1. INTRODUCTION

Scale model testing in wind tunnels has remained a vital step in the development of more efficient, higher performance and cost effective aircraft. This aspect of wind tunnel tests has not changed over the past decades, but data quality, accuracy and connectivity to flight data predictions have become much more important. Performance enhancements between successive stages of modifications to aircraft are getting smaller because of the industry's need to reduce both the cost increments on its product line, and the uncertainties in performance metrics on its newer model releases. This perspective has placed an ever increasing demand on wind tunnel test data quality. Concurrently, market pressures have made it necessary for the industry to shorten the cycle times between new configurations and to ask for a more rapid data generation process in wind tunnels[1]. In recognition of this need to reduce the uncertainty in test data and to shorten the test cycle times, a modernization project was proposed for the NASA Ames Unitary Plan Wind Tunnel (UPWT). Goals for the project were inspired by futuristic projections of wind tunnel testing scenarios and tempered by the realities of funding and schedule limitations.

Initiated in 1988, the modernization project comprised a variety of features including automation, auxiliary facility upgrades, tunnel shell repairs, compressor blade replacement, drive motor refurbishment, data system revisions, and flow quality enhancement systems[2]. Extensive surveys of the flow quality in the test section and measurements of flow characteristics in the rest of the tunnel circuit were subjected to detailed analysis in order to identify the disturbance sources and to determine how those could be eliminated or reduced to improve flow quality. Based on these studies and the flow quality goals prescribed for the project, flow quality

enhancement systems were designed, verified in simulation trials, and implemented after shut–down of the tunnel in April of 1995. Reactivation trials began in late 1998 and included the Integrated Systems Tests. One test phase documented the flow quality in the modernized tunnel for three test section wall configurations: (I) Slots Normal (normal testing configuration, slots open), (ii) Floor Slots Taped (semi-span testing configuration), and (iii) All Slots Taped (a configuration to represent the flow quality that would accrue from acoustic treatment of the wall slots). This paper offers a glimpse of the features of the flow quality enhancement systems and summarizes the current status on flow quality.

2. FLOW QUALITY UPGRADES

NASA Ames 11-by 11-Foot Transonic Wind Tunnel (11-FT TWT) is a variable pressure, closed circuit, internally cooled, continuous operation wind tunnel with an 11-foot square, 22-foot long test section, Fig. 1.

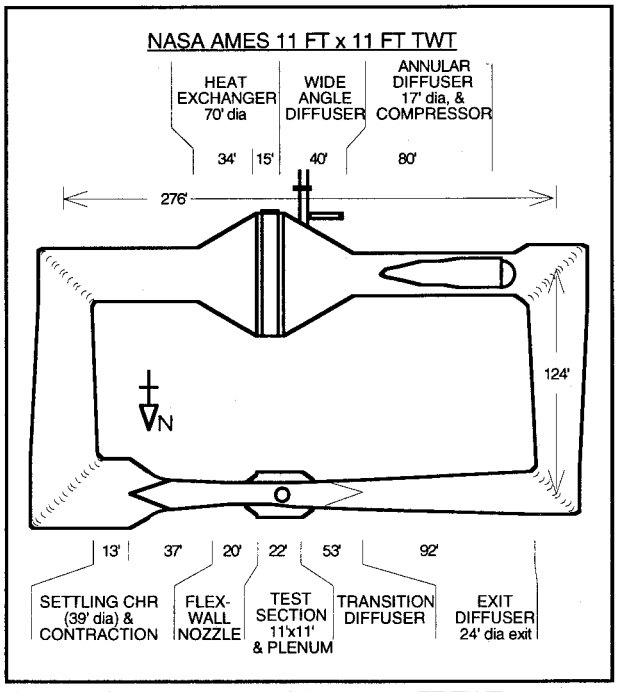

FIG.1 SCHEMATIC OF NASA AMES 11-FT TWT

Slots with baffle inserts run the full length of the test section on all four walls to allow bypass–flow interaction with a large plenum chamber. This offers blockage relief for models, especially at transonic Mach numbers. For any test condition, the level of blockage relief may be varied by altering the deflection settings of four diffuser flaps. These flaps are attached to the exit ends of the four walls of the test section and regulate the suction generated in the plenum chamber.

When refurbishment and upgrades were contemplated more than a decade ago, several areas for improvement were identified based on structural aspects, safety issues, and the potential for test data generation. Generation of test data is a function of a variety of factors, the prominent ones being: the model mounting and positioning system, the data acquisition and processing system, the wall interference correction system, compressor induced flow dynamics, and flow quality. Some of these factors are not mutually exclusive. Degradation in one may affect one or more of the others. It was expected that a fix or upgrade targeted for one of these factors would influence the performance of others and therefore the design of upgrades was studied in greater detail with simulation tests. Detailed studies were undertaken to design upgrades which would reduce the effects of flow dynamics emanating from various parts of the tunnel. When the design of upgrades was complete, the flow quality enhancements to the tunnel consisted of adding two flow conditioning systems to the tunnel circuit – a Turbulence Reduction System (TRS), and a back–leg diffuser flow–smoothing system. Acoustic treatments, especially test section wall noise abatement techniques, were explored, but not implemented because of constraints imposed by the modernization project budget.

The TRS, located in the settling chamber just ahead of the contraction, is made up of a honeycomb followed by two screens, Fig. 2.

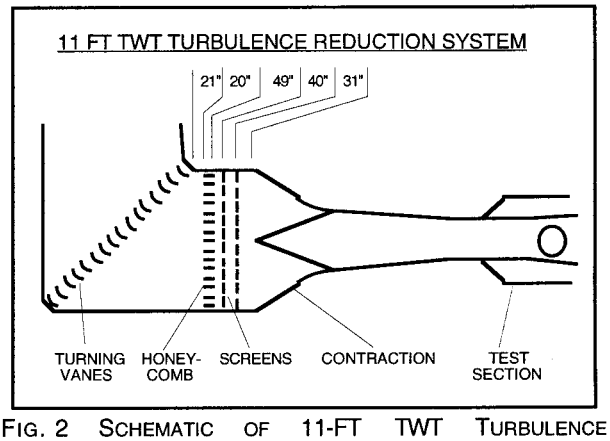

FIG. 2 SCHEMATIC OF 11-FT TWT TURBULENCE REDUCTION SYSTEM

The diffuser flow-smoothing system, placed in the back leg just downstream of the tunnel compressor, has a ring of flow deflector flaps encircling the after–body of the nacelle, followed by a ring of contoured annular turning vanes at the entry to the wide angle diffuser, Fig. 3.

Both these systems were initially configured from design rules and performance data borrowed from existing literature, and then subjected to simulation tests which carefully reproduced the measured entry flow conditions in the tunnel. Results of the simulation tests provided the basis for substantial revisions of the initial design[3,4].

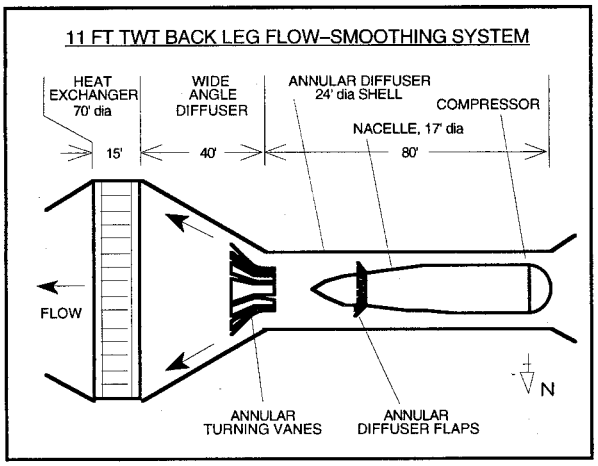

FIG. 3 SCHEMATIC OF 11-FT TWT BACK–LEG FLOW SMOOTHING SYSTEM

Of the two flow conditioning systems, the TRS was expected to reduce the nonuniformities, flow angularities, and turbulence in the flow–field approaching the contraction, thus reducing the turbulence as well as flow angularity in the test section. In contrast, the back–leg diffuser flow smoothing system was meant to eliminate or suppress both the jet–flow and the associated flow recirculation zones in the wide angle diffuser. This would reduce the contributions from those zones to the long–period flow velocity fluctuations which affect Mach number stability in the test section.

2.1 TURBULENCE REDUCTION SYSTEM

Using existing correlations, many TRS designs with different combinations of flow conditioning honeycombs and screens were examined in order to select a smaller set of design options for simulation testing.

Flow quality measurements collected in the tunnel prior to the modernization were used in defining the velocity profile distortions and turbulence levels entering the settling chamber area designated for the TRS. The profile, characterized both by its deviation from uniformity and by its slope variation across the flow passage, was known to be important because of its potential to generate turbulence further downstream.

Another aspect of the design was the attenuation properties of honeycombs and screens. It was noted that performance correlations available from existing published literature largely referred to elements that were carefully fabricated to tight specifications. However, the proposed installation in the 11-FT TWT would reflect production tolerances that apply to large panels assembled with joints across edges of standard panels to fill the entire 38-foot diameter cross section. Such imperfections were expected to not only adversely affect attenuation properties but also to produce higher levels of self–generated turbulence and were therefore deemed important.

The nature of the profile deficits, the scale lengths associated with the slope variations, and the need to characterize the performance of full–scale production–quality TRS elements were such that simulation testing was considered a necessary step before finalizing the design. It was clear that all of the profile properties could not be reproduced in their entirety in the limited size of a scaled–down test apparatus. A stream–tube modeling concept was therefore evolved for simulation tests. Profile properties and turbulence levels in different stream tubes across the tunnel flow passage were individually generated in the simulation apparatus and the attenuation properties of the selected TRS options were measured. Although the highest values of profile deficits, slopes and turbulence could be treated as the deciding factors for arriving at a successful TRS option, it was important to measure the performance at less severe conditions in order to follow the stream tubes and map the projected profiles in the test section. The profiles in the test section would then be the basis for arriving at an optimum TRS design to meet the flow quality goals in the core. Clearly, lower flow quality levels were acceptable for the near–wall regions. However, in order to make the final choice, it was desirable to

have an understanding of what the levels would be in the core region and what the trade–offs would be between costs and performance for further additions to the TRS. The simulation tests, which provided the desired database, were discussed in detail by Murthy, Kmak and Koss[5].

The selected design configuration of the TRS was composed of a honeycomb followed by two screens placed in a compact layout to accommodate the short length of the existing settling chamber, Fig. 2. The honeycomb installation is made up of fifteen 13-by 8-foot panels; some trimmed at the outer edges to fit the 39-foot diameter circle of the tunnel shell. The panels were interconnected with butterfly shaped connectors to fill the shell of the settling chamber[3]. Each panel was built from 0.010-inch thick stainless steel sheet material to produce 1-inch hexagonal cells, 20 inches deep. The screen installation was built up from 45-foot wide by 8-foot high screen panels trimmed to fit the 39-foot diameter tunnel shell. Sections were carefully joined by welding every pair of matching wire ends to preserve the continuity of every mesh along the joint. Screen panels contain 0.041-inch diameter wires in a self–locking weave of 6 wires/inch. The honeycomb installation was firmly attached to the tunnel shell to produce a fixed–end constraint, whereas each screen installation was simply supported from its own ring of spring–tensioned mounts grounded to the shell.

2.2 BACK–LEG FLOW SMOOTHING SYSTEM

Flow leaving the compressor in the back–leg (drive–leg) of the tunnel circuit passes into a tandem diffuser system consisting of an annular diffuser formed by a nacelle centered inside a uniform diameter shell followed by a wide angle diffuser ending in a heat exchanger. This flowfield was known to be complex because of the variability in the velocity profile emerging from the compressor at different tunnel Mach numbers. It was also interactive in the sense that the flow instabilities produced by the annular and wide angle diffusers would react to the flowfield of the other at the common interface. The complexity and the interdependency of the total flowfield were deemed substantial and together frustrated any attempt to idealize it as individual parts for studies of treatment options. Likewise any option for a flow smoothing system, in order to be cost–effective, needed to be derived as a coupled solution for the entire diffuser system, not as a system composed of two independent parts each designed for its host diffuser.

Measurements of velocity profiles at various stations along the back–leg diffuser system had shown that velocity deficits near the walls of the outer shell of the annular diffuser were substantial and triggered the early formation of jet–flow at the entry to the wide angle diffuser. This jet–flow was deflected outwards in front of the heat exchanger like the spread of a stream impinging on a plate, and then proceeded to form large scale flow recirculation zones along the walls of the wide angle diffuser. Pulsations and rotating instabilities induced by the recirculation zones were expected to be one of the sources of moderate–to–long period variations in test section Mach number.

In recognition of the complexity and the interactive nature of the flowfield in the two diffusers, it was decided that a search for flow treatment options should be performed in a simulation apparatus. A scaled down replica of the geometry of the two diffusers was built and inserted into the circuit of an existing research facility. A set of flow altering devices was designed and built for placement at the inlet of the apparatus in order to control the profiles at the entry to the first diffuser. The heat exchanger installation was simulated by installing a flow resistance device composed of perforated plates fitted into frames at the exit of the wide angle diffuser.

Initial tests in the simulation apparatus were aimed at reproducing the basic features of the flow entering the diffuser system and verifying the profiles at various stations along the length for conformity with the profiles measured in the primary tunnel. Adjustments were made to the inlet flow control devices and the heat exchanger simulator until the profiles in the simulation facility matched the profiles in the tunnel. Once these adjustments were completed, the next phase of evaluating flow manipulation options began with the primary goal of eliminating or substantially shrinking the recirculation zones in the wide angle diffuser.

A large matrix of coupled systems were tried, with many options of flow conditioning devices in the annular diffuser paired one at a time to an equally large number of options in the wide angle diffuser. Devices reported in literature were the initial choices, ranging from vortex generators and flow control rods in the annular diffuser to radial splitter

vanes, large scale vortex generators, double delta wing vortex generators, nested straight cones, nested contoured cones, moderate–angle diffuser insert, and screens in the wide angle diffuser. For practical reasons, especially in view of the complexity of installation as retrofits, the devices in the wide angle diffuser were restricted in axial length to one quarter of the total length of the diffuser. None of the pairs of options produced acceptable results. Either the recirculation zones remained large, or high velocity jet flow remained somewhere in the flowfield. It was clear that the solution had to be more robust and respond to the variability in the peaky profile shapes of the flow entering the annular diffuser.

A new concept was evolved to produce a satisfactory flow smoothing system. Simply stated, the concept envisioned a device on the nacelle after–body which would direct the higher momentum core flow toward the outer walls, followed by a device in the wide angle diffuser which would turn this higher momentum flow toward the diverging walls. The chosen device was a ring of flow deflecting flaps on the nacelle and an annular ring of turning vanes at the entry in the wide angle diffuser, Fig. 3. The annular diffuser flaps on the nacelle were discrete with finite gaps on the sides of every flap to promote bleed flow into the wake region and prevent it from growing into a large recirculation zone. The annular turning vanes in the wide angle diffuser were also discrete with finite gaps in order to allow for controlled interaction between the wall–flow region turned by the vanes and the interior core–flow region passing along the tunnel centerline. The interaction across the gaps would ensure that the two parts of the flow leaving the annular turning vane region, namely the interior flow and the outer wall–flow, did not generate shear flow instabilities which may have the potential to merge into a large recirculation zone.

Extensive trials were performed and detailed flowfield measurements were taken in order to obtain a parametric database of the geometrical variables of both the annular diffuser flaps and the annular turning vanes. Measurements of velocity profile and wall–static pressure distribution, combined with flow visualization using wall–mounted tufts and traversed tuft–wands, provided the basis for making judgements on the performance of the dual system. Unfortunately, the number of variables in this parametric evaluation was extensive and the study was halted by the realities of the project timeline. Although the database was not complete in all respects, it was enough to select a valid system that offered substantial improvements in the flow diffusion process.

In the final design configuration, the flow deflector flap system contained twenty identical flaps set to a nominal incidence angle of 40° and distributed evenly on the after–body of the nacelle with equal gaps between flaps. The annular turning vane system was composed of twelve flat–plate vanes shaped to capture the outer half of the incoming flow and deflect it to pass along the walls of the wide angle diffuser. These vanes were installed with leading edges nominally 5-feet off the wall and spaced to leave equal gaps between them.

3. FLOW QUALITY INSTRUMENTATION

As a part of the Integrated Systems Tests (IST), detailed flow measurements were performed with instrumentation placed at several locations in the tunnel circuit. Pitot rakes stretching across the entire flow passage and wall–static taps at several stations in the back leg provided data on flow–field improvements accomplished by the diffuser flow–smoothing system. These improvements contribute to flow quality, but do not directly provide a measure of the flow quality gains in the test section, and therefore will not be discussed further in this paper.

Test section flow quality was directly quantified with flow sensing probes distributed on an 8-Foot span rake mounted on a sting support system, Fig. 4. The probes on this rake were distributed among 21 stations along its span and consisted of: a single flow angularity probe with a 5-hole sensor at the tip and static pressure ports on the aft–body, ten turbulence sensing probes with either single–element hot wire sensors (u') or selectively oriented two–element X-wire sensors (v', w'), and two acoustic sensing cone probes with total and static pressure transducers (Pt', p'). The mounting of every probe, with the exception of the flow angularity probe, was adjusted to place the sensor at tunnel station 185 (distance from test section entry = 185 inches).

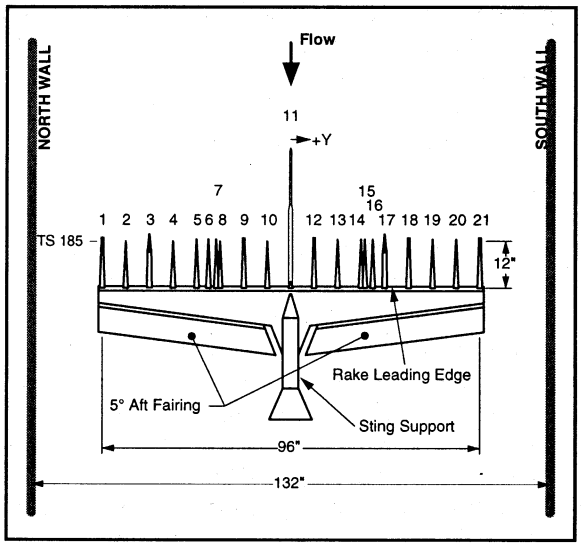

SLOT (Y/W) W=11 FT	MEASURED FLOW VARIABLE
1 (-0.364)	Tt
2 (-0.319)	u'
3 (-0.273)	Pt' and p'
4 (-0.228)	u'
5 (-0.182)	v'
6 (-0.159)	
7 (-0.144)	w'
8 (-0.137)	u'
9 (-0.091)	Tt
10 (-0.046)	u'
11 (0.000)	Flowangle, Pt, p

SLOT (Y/W) W=11 FT	MEASURED FLOW VARIABLE
12 (0.046)	Tt
13 (0.091)	u'
14 (0.137)	u'
15 (0.144)	
16 (0.159)	u'
17 (0.182)	Pt' and p'
18 (0.228)	Tt
19 (0. 273)	u'
20 (0.319)	
21 (0.364)	Tt

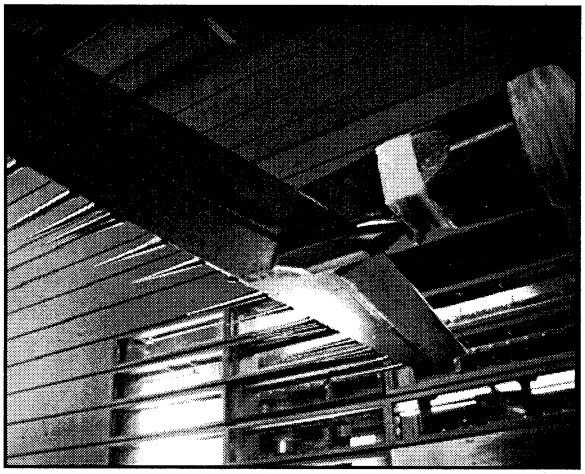

Fig. 4 A Schematic and a Photograph of the 8-Foot Span Instrumented Rake

3.1 FLOW ANGULARITY PROBE

Flow Angularity data were obtained from a 5-hole probe with holes arranged on a 40° conical nose and an additional set of static pressure sensing taps arranged on its aft-body, Fig. 5. All pressure taps were carefully drilled to provide a 0.015-inch diameter exposure to the flow. This probe was mounted on a standoff at the mid-span station of the 8-Foot rake placing it 6.625 inches below the rake. The static pressures on the conical nose were located at tunnel station 164.1, the total pressure port at TS 163.6 and the reference static pressure on the aft-body at TS 169.5. Differences in pressures were measured with highly sensitive, temperature compensated, DRUCK® differential pressure transducers housed in a temperature controlled chamber placed inside a fairing on the rake. The total pressure was teed off to a PAROSCIENTIFIC absolute pressure transducer, to be used as a local flow reference.

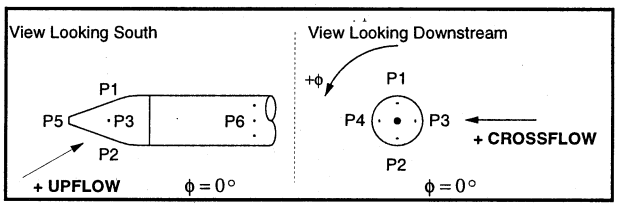

FIG. 5 SCHEMATIC OF THE 5-HOLE CONE PROBE

3.2 TURBULENCE PROBES

Turbulence data were acquired from several hot wire probes mounted at selected stations on the rake. Sensors were 5 micron diameter tungsten wires welded to prongs spaced approximately 1.2 mm apart. These were operated from a 16-channel TSI®–IFA-100 constant temperature anemometer system. Each wire element was operated with its own anemometer bridge unit and individually optimized for frequency response characteristics by adjusting a pair of compensation settings against a square wave test signal. Outputs from the bridge units were passed through an equal number of signal conditioning units which allowed independent selection of high–pass and low–pass frequency windows.

3.3 ACOUSTIC PROBES

Acoustics data were collected from two 10° apex–angle cone probes each with miniature pressure transducers mounted in two places, one set into the tip of the cone to sense total pressure fluctuations and the other buried flush into the conical surface, roughly 1.7 inches from the nose–tip, to sense static pressure fluctuations. Both transducers were the differential type, chosen to offer high accuracy at all Mach numbers. Reference pressures were generated from a static port on the cone surface and a total pressure pitot probe mounted off the surface at the base of the cone. A damping volume and a flow–restricting

narrow passage were added to the plumbing of each reference port in order to suppress fluctuations in the reference pressure. The transducers were operated from standard power supplies, and signals were amplified before transmission to the data system.

3.4 FLOW QUALITY SURVEYS

The 8-Foot rake was traversed vertically between the top and bottom walls of the test section over a range of y/H = –0.38 to 0.28. Test conditions were monitored with a total pressure probe in the settling chamber downstream of the screens and a static pressure probe in the plenum chamber. Through most of the flow quality surveys, the test section exit diffuser flaps remained at the "normal" setting and the wall slots contained "standard" baffle inserts, a configuration used in the past for all full–span models. A semi–span testing configuration associated with floor–mounted models was surveyed after securely taping over all of the slots on the floor. A third "high flow quality" configuration, which offers a look at the improvements in flow quality that can be expected from acoustic suppression treatment of wall slots, was established by taping all the wall slots of the test section. Results of flow quality surveys made with this last configuration are expected to provide advocacy for future upgrades relating to flow quality as well as wall interference correction systems.

3.5 DATA ACQUISITION SYSTEMS

Pressure signals from the differential transducers of the flow angularity probe were routed into the Standard Data System (SDS), Fig. 6. Turbulence signals from the hot wire constant temperature anemometer system and acoustic signals from the pressure transducer processing system were processed through three parallel dynamic signal analysis and acquisition system paths. The first path utilized a set of root mean square (RMS) meters with adjustable time capture to generate steady state outputs equal to the total RMS values and supplied those to SDS for routine acquisition. A second path through a PC-based Hewlett Packard (HP®) MODEL-3565 dynamic data system offered the option of monitoring the spectral content of chosen channels in real time to detect sensor problems or to identify any flow related problems to be investigated further. The third path delivered the signals to a Hewlett Packard (HP®) MODEL-E1433A dynamic data system operated with LMS® software written for archival and detailed analysis purposes. The User Programming Application (UPA) feature of the LMS® system made it possible to add a custom program for decomposition of the signals into spectral content, primarily Power Spectral Density (PSD) and 1/3 Octave presentations. The custom package also incorporated calculations for derivation of lateral turbulence components from the X-wire signal pairs.

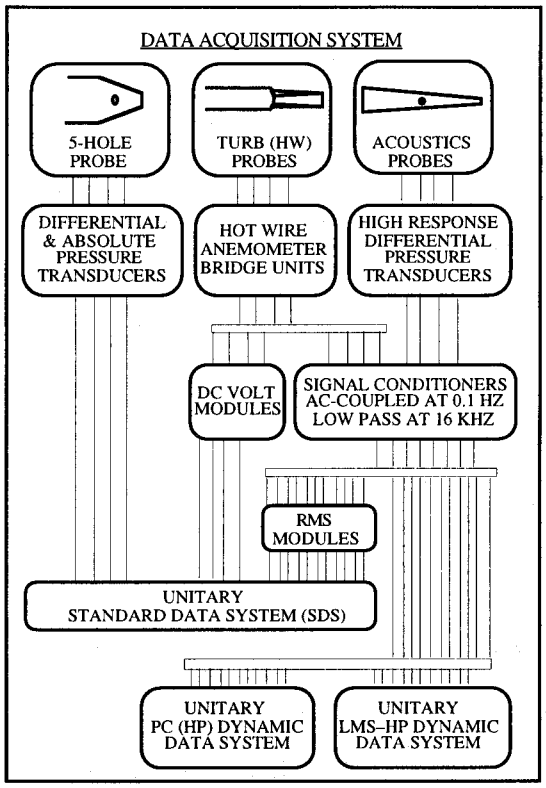

FIG. 6 BLOCK DIAGRAM OF DATA ACQUISITION SYSTEMS

4. FLOW ANGULARITY DATA

Established procedures were used for calibrating the 5-Hole Probe in the pitch and yaw planes. Calibration constants derived from calibration runs were applied to the measured pressure data for various tunnel conditions to document the flow angularity properties of the tunnel. Data acquisition and averaging durations were carefully selected and verified to achieve high resolution and accuracy in flow angle measurement.

4.1 CALIBRATION OF THE 5-HOLE PROBE

The 5-hole probe was instrumented to provide simultaneous measurements of the local UPFLOW and CROSSFLOW as defined in Fig. 5 and derived

by the equations similar to the ones listed below for probe rotation angle ø=0°.

UPFLOW = UK1 x CPTU + UK0 x KPHI – Alpha

CROSSFLOW = CK1 x CPTC + CK0 x KPHI + Beta

where the coefficients, UK1, UK0, CK1, and CK0 are determined from the probe calibration.

The non-dimensional pressure coefficients, CPTU and CPTC, are derived from cone pressures by,

$$CPTU = \left(\frac{P_1 - P_2}{P_6 - P_5}\right) \times KPHI$$

$$CPTC = -\left(\frac{P_3 - P_4}{P_6 - P_5}\right) \times KPHI$$

KPHI is a probe rotation angle (ø) correction factor to account for the rotational settings of the probe,

KPHI = 1, for ø = 0°
= 1, for ø = 90° (with UPFLOW and CROSSFLOW equations switched)
= –1, for ø=180°

The 5-hole probe was calibrated in the test section (Slots Normal) for Mach numbers in the range 0.2 to 0.95 at a total pressure of 3180 psf to obtain the probe sensitivity coefficients and offsets in the pitch and yaw planes.

The calibration procedure consisted of pitching the probe for three probe roll orientations, ø=0°, ø=180° and ø=90°. At each pitch setting, two cone pressure differentials, P_1-P_2 and P_3-P_4, as well as the differential between the probe static reference and the total pressure, P_6-P_5, were measured using differential pressure transducers. The differential pressures were used to compute the two non-dimensional pressure coefficients, CPTU and CPTC. The probe total pressure, P5, was measured using an absolute pressure transducer. The upflow coefficients, UK1 and UK0, and the upflow component of the flow angularity, UPFLOW, were derived from a plot of CPTU vs. Probe Incidence Angle using the ø=0° and ø=180° runs. Among the crossflow coefficients, the slope CK1 was derived from the plot of CPTC vs. Probe Incidence Angle for the ø=90° runs. The probe offset CK0 and the yaw component of the flow angularity, CROSSFLOW, were derived from the CPTC data for zero yaw settings collected over the entire range of pitch sweeps at ø=0° and ø=180°.

Figure 7 is a plot of CPTU vs. Probe Incidence Angle at Mach =0.8, PT = 3180 psf and angle range = ±1° for the upright run (ø = 0°) and the inverted run (ø = 180°), with the sign of the CPTU switched for the last orientation.

Thin lines represent a least squares fit of the data. Also shown on this plot, is the mean-line, which represents the true probe calibration curve and is the average of the upright and inverted curve-fits. The inverse slope of the mean line, (ΔAlpha/ΔCPTU), defines the probe sensitivity coefficient, UK1. The difference in intercepts between the curve-fit of the upright run and the mean-line is the offset, UK0. The intercept of the mean line relative to the origin of the coordinate system, (0,0), is the upflow angularity, UPFLOW, at the probe location in the flowfield, with the sign switched.

$UK0 = K0_{ø=0°} - K0_{Mean\text{-}line}$

$UPFLOW = - K0_{Mean\text{-}line}$, at z/H = -0.085

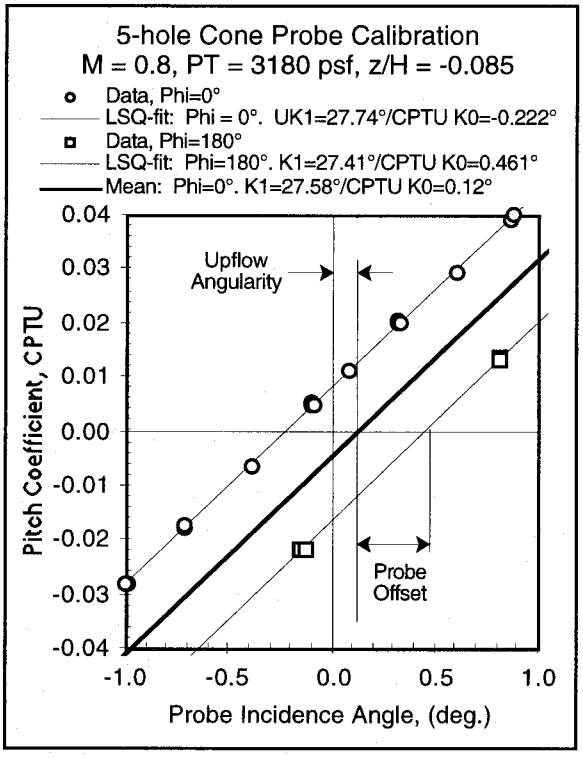

FIG. 7 5-HOLE PROBE PITCH COEFFICIENT CALIBRATION

Figure 8 is a plot of CPTC vs. Probe Incidence Angle at Mach =0.8, PT = 3180 psf and angle range = ±1° for ø = 0°, ø = 90° and ø = 180°, with the sign of CPTC switched for the last orientation.

The line for ø=90° is a least squares line–fit for the data, and its inverse slope (ΔAlpha/ΔCPTC), defines the probe sensitivity coefficient, CK1. This value was then applied to the zero–alpha

intercepts of the individual line–fits of CPTC for ø=0° and ø=180° to obtain the CROSSFLOW angularity in the local flow and the probe offset (CK0). The individual line–fits of CPTC are shown as thin lines in Fig. 8 to represent the data for zero yaw settings over the entire range of pitch sweeps. The mean line, shown as a thick line, is the average of the line–fits for ø=0° and ø=180°, and therefore gives the true intercept for the calibration line.

$$CK0 = CK1 \times \Delta CPTC_{\text{mean line vs. } ø=0^\circ \text{ line}}$$

$$CROSSFLOW = CK1 \times \Delta CPTC_{\text{mean line vs. } (0,0)^\circ \text{ at } z/H = -0.085}$$

It may be noted here that the signs of the intercepts pertaining to flow angularity and probe offset were carefully tracked all the way through the data for different probe rotations. The final check on the flow angularity data reduction equations and the sign convention was accomplished by computing the UPFLOW and CROSSFLOW angularity components from the data for zero–angle settings of the probe in both the probe–upright and probe–inverted runs. Verification was complete when the data reduction equations produced the same results for both cases.

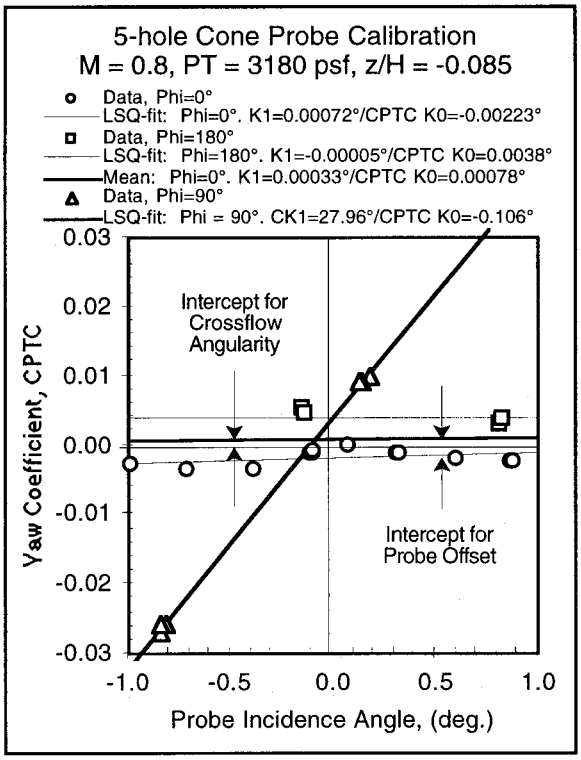

Fig. 8 5-Hole Probe Yaw Coefficient Calibration

4.2 FLOW ANGULARITY LEVELS

Figures 9-14 present the vertical variation of the flow angularity for the three test section configurations; slots normal, floor taped, and all slots taped. Pre-modernization data, obtained from a similar 5-hole cone probe, is also included for the normal and floor taped configurations for comparison. Limits imposed by the survey apparatus on the present test prevented measurements above z/H = 0.23.

FLOW ANGULARITY FOR SLOTS NORMAL (NORMAL TESTING CONFIGURATION)

The UPFLOW profile for the slots normal configuration, Fig. 9, shows a uniform, virtually zero–angularity core region, with an increased flow angularity near the floor. The higher values (negative) of UPFLOW for positions below z/H = -0.27 is caused by the flow passing through the slots aided by the suction in the plenum. As one would expect, the magnitude of the flow angle increases with proximity to the floor. Present data exhibits good agreement with pre-modernization data for heights above z/H > -0.06. Near z/H = -0.2, the profile for the pre-modernization data exhibits a spike, showing hints of a perturbation of -0.2° in the flow. This feature is not present in the IST data.

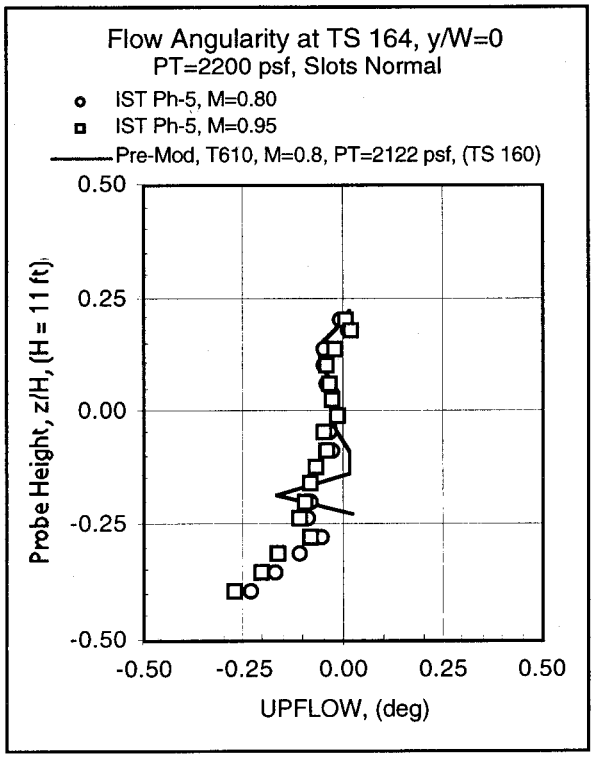

FIG. 9 VERTICAL PROFILE OF UPFLOW, SLOTS NORMAL

The CROSSFLOW profile, Fig. 10, appears to meander from floor to ceiling, with a hint of symmetry about the tunnel centerline, but exhibits no significant trend to warrant an explanation. CROSSFLOW angles in pre-modernization data reveal a significant perturbation of 0.3° also near z/W = -0.2. Again, this feature is entirely absent in the IST data. This is an expected result from the flow conditioning systems introduced in the modernization effort.

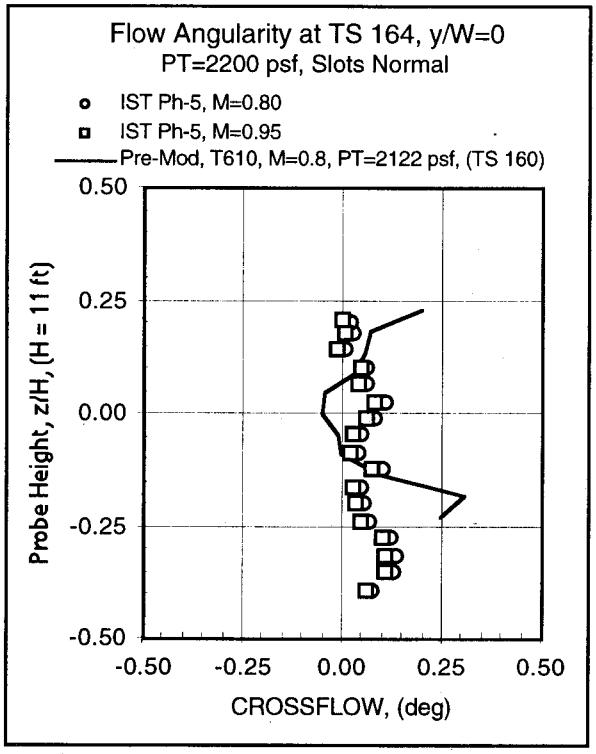

FIG. 10 VERTICAL PROFILE OF CROSSFLOW, SLOTS NORMAL

The effect of Mach number on the flow angularity appears slight. The shifts in the UPFLOW and CROSSFLOW profiles do not change significantly with Mach number and are mostly within ±0.03°.

The most obvious improvement in the flow angularity resulting from the addition of the TRS, or more specifically the honeycomb, is the elimination of the large flow angularity perturbations present in the pre-modernization flow field. Pre-modernization surveys showed a large perturbation in the flow angularity centered near z/H = -0.2. IST data clearly show that this feature is no longer present.

FLOW ANGULARITY FOR FLOOR SLOTS TAPED (SEMI–SPAN TESTING CONFIGURATION)

Taping the floor slots causes flow near the floor to migrate towards the tunnel centerline along the path of least resistance. The resulting UPFLOW profile, Fig. 11, shows a reduction in the overall gradient over the traverse range with a significant decrease in the UPFLOW near the floor. A noticeable shift to higher UPFLOW angles for M=0.95 is indicative of the readjustment the flow must make in order to overcome the loss of blockage relief on the floor. This readjustment becomes more acute at higher Mach numbers as the flow near and behind the 8-Ft rake approaches sonic speeds and alters the share of plenum suction imposed by each of the four diffuser flaps.

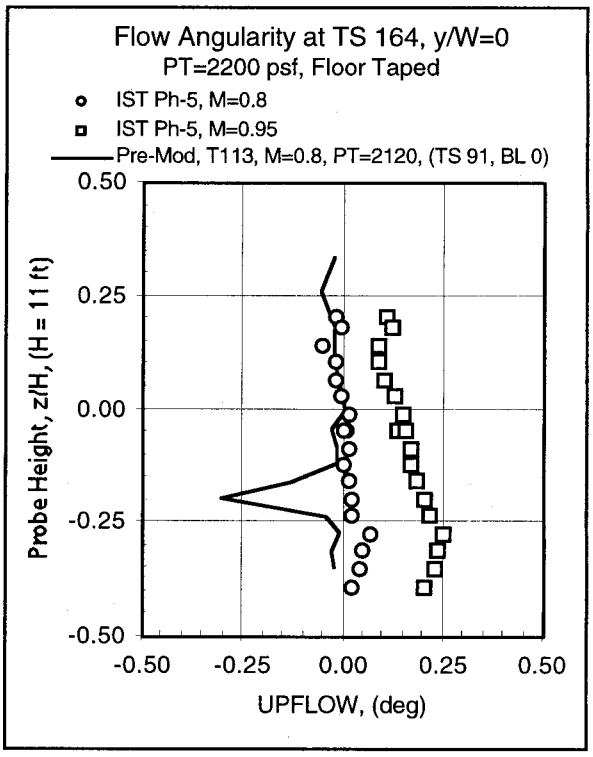

FIG. 11 VERTICAL PROFILE OF UPFLOW, FLOOR SLOTS TAPED (SEMI–SPAN TESTING CONFIGURATION)

The effect of taping the floor slots on the CROSSFLOW profile, Fig. 12, is a slight shift in the magnitude and no significant change in the variations with height. The profiles are very similar to the results obtained with the slots normal. This is expected because the flow symmetry in the yaw plane was unchanged.

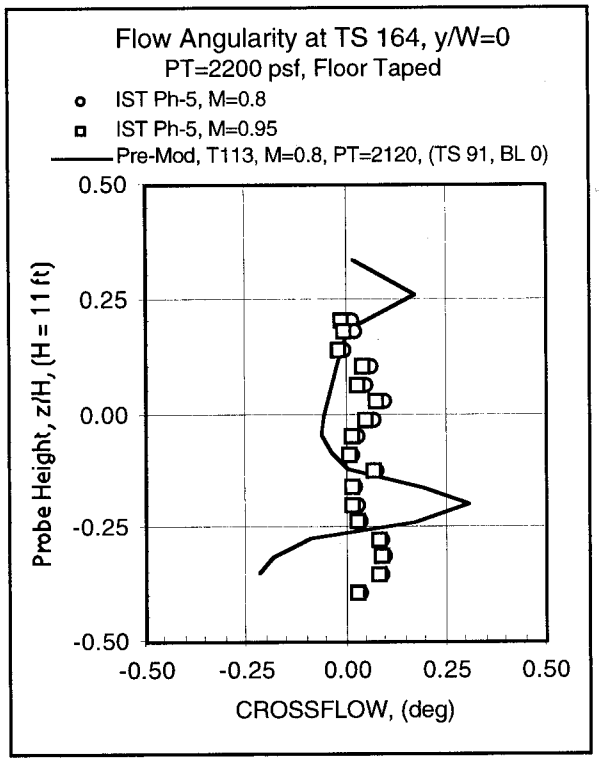

FIG. 12 VERTICAL PROFILE OF CROSSFLOW, FLOOR SLOTS TAPED (SEMI–SPAN TESTING CONFIGURATION)

Here again, as in the Slots Normal configuration, the most obvious improvement in the flow angularity resulting from the addition of the TRS is the elimination of the large flow angularity perturbations present in the pre-modernization flow field near z/H = -0.2. At M=0.8, the magnitude of this variation was on the order of 0.3° in UPFLOW and 0.3° in CROSSFLOW. As with the slots normal configuration, present data clearly show that this large flow angle perturbation is no longer present.

Another feature of the pre-modernization data is the level of perturbation above the centerline. Pre-modernization data which extended to z/H = 0.35 indicate that the perturbation phenomenon existed above the centerline as well, although the magnitudes appear to be smaller, Figs. 11 and 12. However, the coarseness of the survey above centerline, every 10 inches as opposed to every 6 inches, may not have been sufficient to capture the profile in detail. In any case, there is no data for the upgraded tunnel for positions above z/H = 0.2, but it is fair to conclude on the basis of the IST data below the centerline that no perturbation is likely to exist above the centerline.

FLOW ANGULARITY FOR ALL SLOTS TAPED (HIGH FLOW QUALITY TESTING CONFIGURATION)

Taping all four walls prevents any flow from entering the plenum, and the wall boundary layer build-up causes the flow near the walls to migrate towards the centerline. This effect is seen in the UPFLOW profiles, Fig. 13.

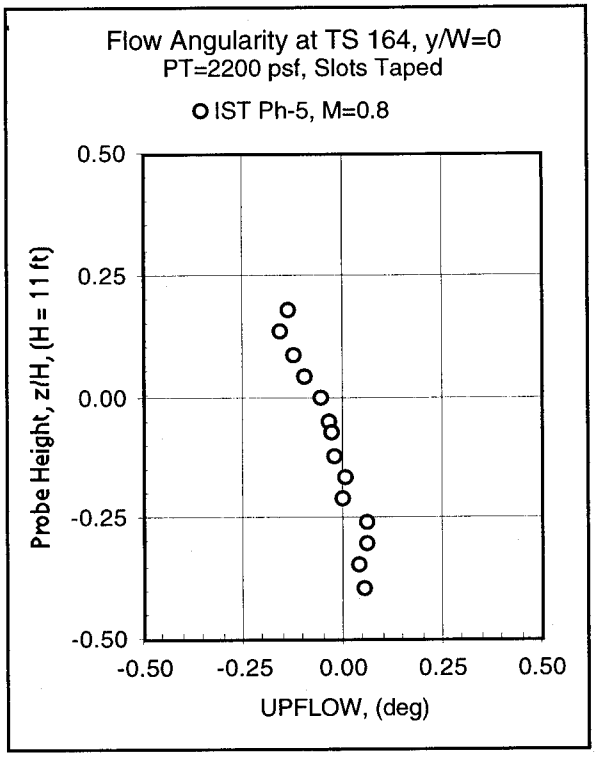

FIG. 13 VERTICAL PROFILE OF UPFLOW, ALL SLOTS TAPED (HIGH FLOW QUALITY LIMIT CONFIGUARATION)

The CROSSFLOW profiles show even smaller variations with height evident in comparison to both slots normal and floor taped configurations, Fig. 14. The profile is flat except very close to the wall where there is a slight perturbation near z/H = -0.36. The reduced waviness in the CROSSFLOW profile suggest that the flow through the slots have a direct influence on the CROSSFLOW profile, to the extent of introducing a slight waviness in the slots normal and floor taped cases.

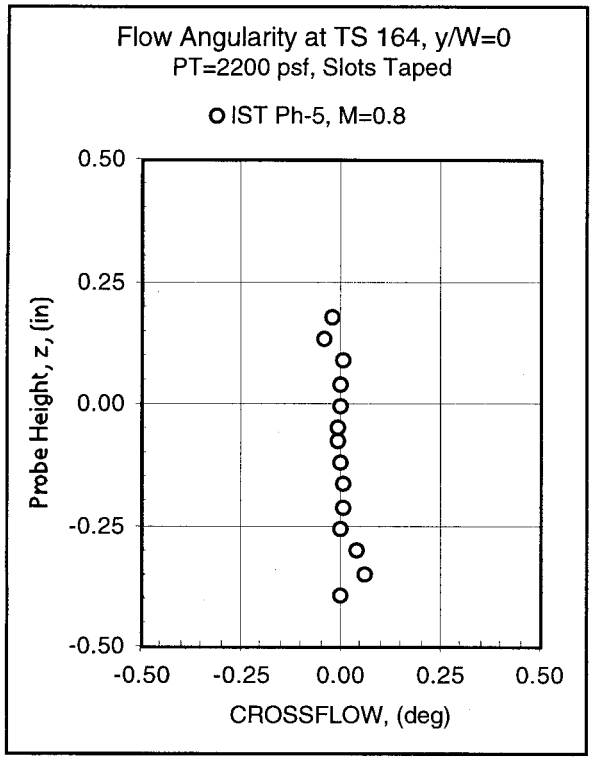

Fig. 14 Vertical Profile of Crossflow, All Slots Taped (High Flow Quality Limit Configuration)

4.3 MACH NO. EFFECTS ON FLOW ANGULARITY

The effect of Mach number on flow angularity is summarized in Fig. 15-20 for the three tunnel configurations. These data are presented in four different sets: one for z/H=-0.05, a second set for z/H=0, a third set showing the averaged angularity level for the range z/H = -0.23 to 0.23, and the last set to display an average over the entire vertical traverse over z/H = -0.38 to 0.28.

Data for z/H = -0.05 were directly measured with the 8-ft span rake positioned at the centerline while the Mach number was varied at selected tunnel total pressures. Also included in this set are measurements picked from vertical traverse data for the specific z/H = -0.05 location which serve to demonstrate the excellent data repeatability manifested during the entire test. The second data set for z/H = 0 was linearly interpolated from the vertical traverse measurements above and below the centerline. The third and the fourth data sets are simply averages extending over the stated range of traverse.

MACH NO. EFFECTS FOR SLOTS NORMAL

Figures 15 and 16 show the flow angularity for the normal test section configuration. The lines represent averages of the data at z/H = -0.05 over the Mach number range, 0.6 ≤ Mach ≤ 0.95, which are –0.039° for UPFLOW and 0.049° for CROSSFLOW. These results demonstrate that the flow angularity remains virtually invariant with Mach number.

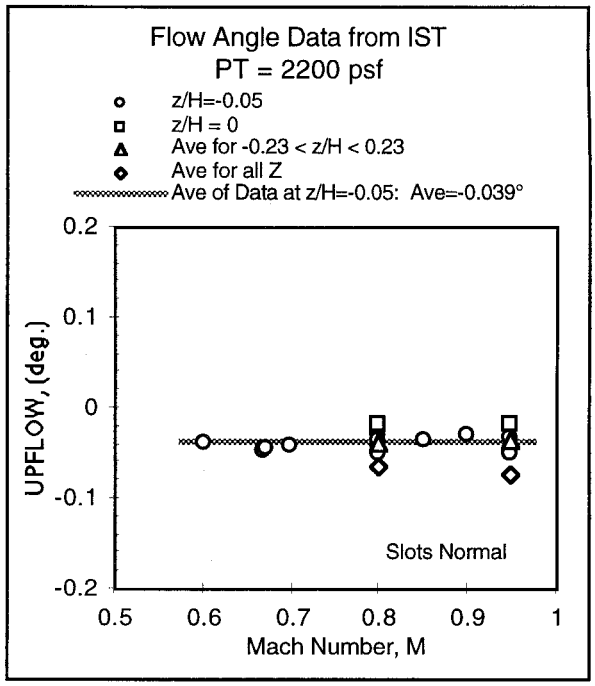

FIG. 15 MACH NUMBER EFFECTS ON UPFLOW NEAR TUNNEL CENTERLINE, SLOTS NORMAL

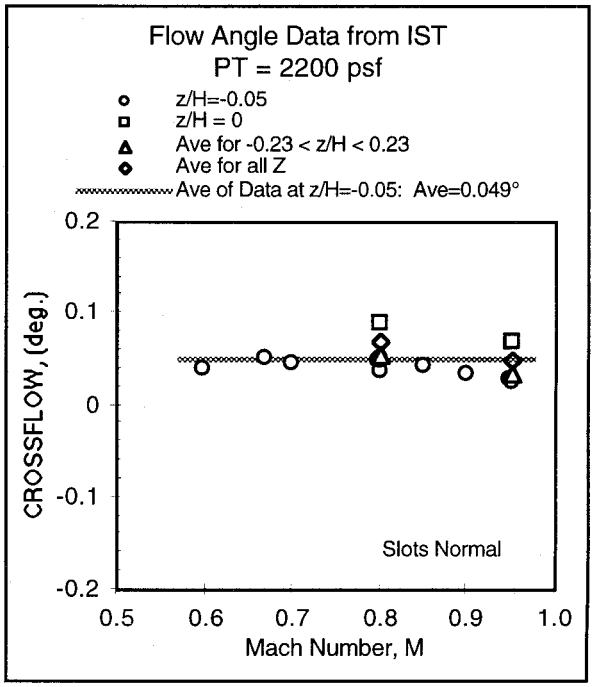

FIG. 16 MACH NUMBER EFFECTS ON CROSSFLOW NEAR TUNNEL CENTERLINE, SLOTS NORMAL

MACH NO. EFFECTS FOR FLOOR SLOTS TAPED

For the Floor Slots Taped configuration, an increase in UPFLOW with Mach number is evident in the data, Figs. 17 and 18. This trend is perhaps caused by the loss of blockage relief on the floor, a factor which becomes increasingly critical at higher Mach numbers and causes the flow to take the least resistance path towards the ceiling. The nature of this trend may be captured by a curve-fit shown in Fig. 17. In contrast, the CROSSFLOW displays a mild decreasing trend perhaps due to a mismatch between the extra plenum suction drawn by the two side walls while compensating for the loss of floor blockage relief.

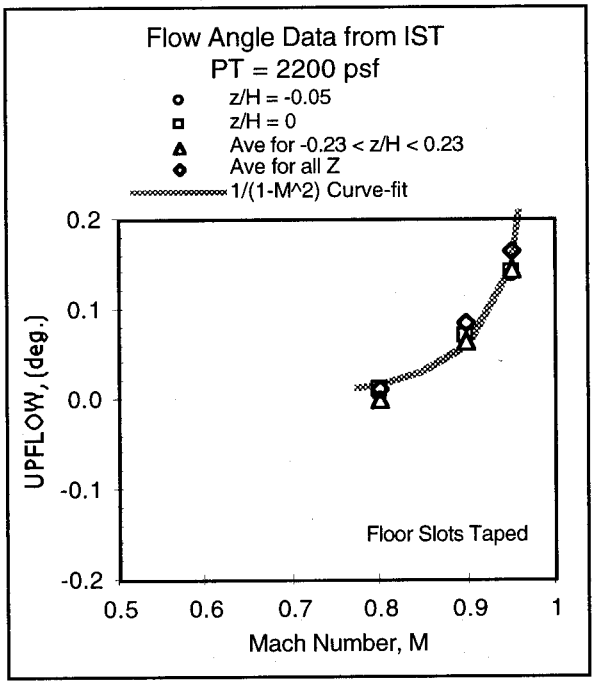

FIG. 17 MACH NUMBER EFFECTS ON UPFLOW NEAR TUNNEL CENTERLINE, FLOOR SLOTS TAPED

MACH NO. EFFECTS FOR ALL SLOTS TAPED

For the All Slots Taped configuration, the flow angularity variation with Mach number is similar to the slots normal configuration, Figs. 19 and 20. Averages for the data at z/H = -0.05 for the UPFLOW (-0.044°) and the CROSSFLOW (-0.026°) are represented by the solid line and compare well to values for the slots normal configuration. This is to be expected because the symmetry of the test section wall configuration, despite the wall boundary layer effects introduced when taping the floor, should result in similar flow angularity levels at the tunnel centerline.

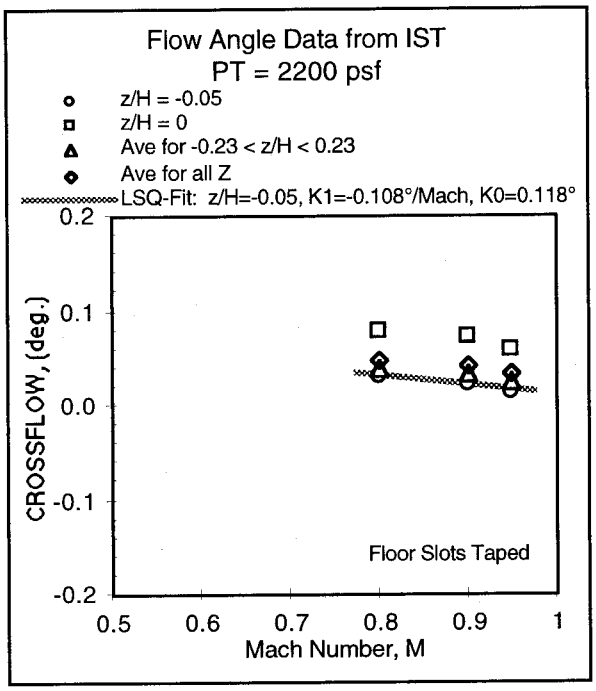

FIG. 18 MACH NUMBER EFFECTS ON CROSSFLOW NEAR TUNNEL CENTERLINE, FLOOR SLOTS TAPED

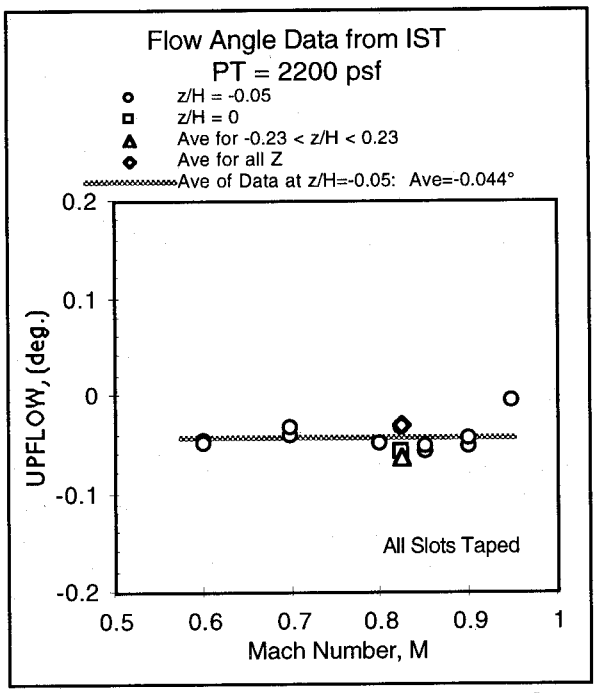

FIG. 19 MACH NUMBER EFFECTS ON UPFLOW NEAR TUNNEL CENTERLINE, ALL SLOTS TAPED

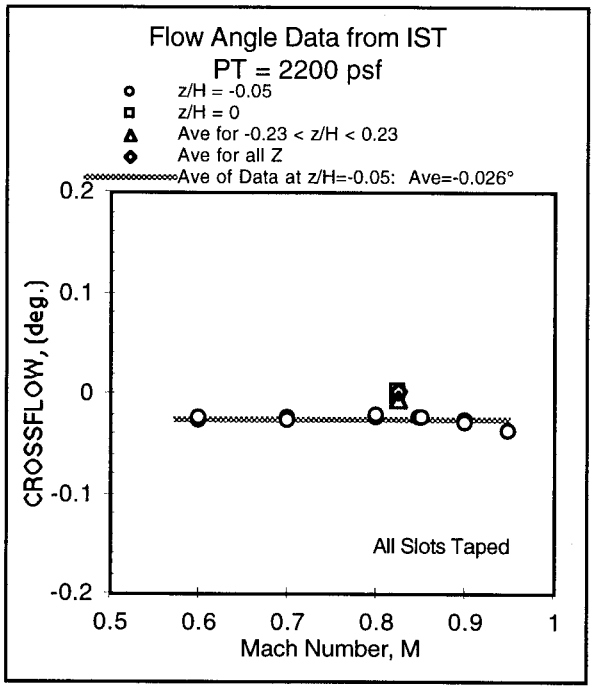

FIG. 20 MACH NUMBER EFFECTS ON CROSSFLOW NEAR TUNNEL CENTERLINE, ALL SLOTS TAPED

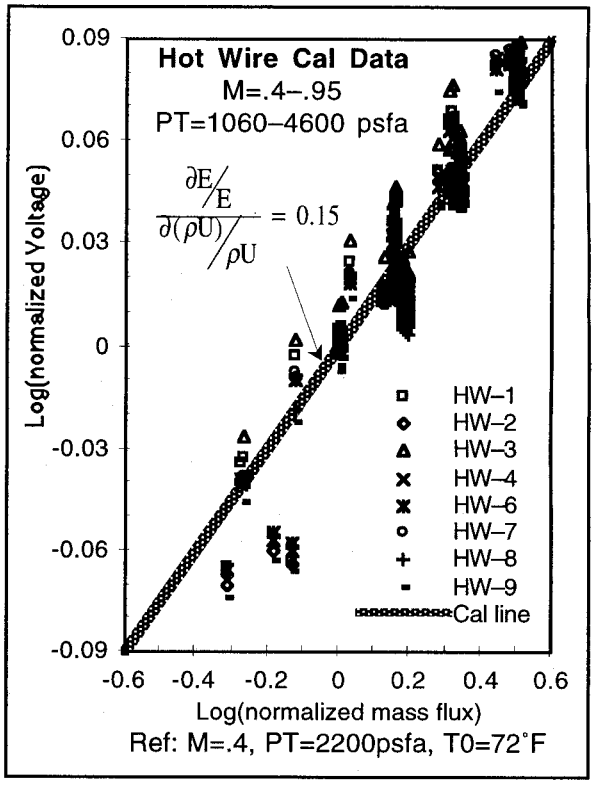

FIG. 21 CHARACTERISTICS OF HOT WIRE PROBES

5. TURBULENCE DATA

Standard procedures were used in reducing data from the hot wire probes. Voltage–turbulence sensitivity values for the different probes were derived from established calibration laws and found to be virtually invariant between probes. Thus, all hot wire measurements were reduced with a single sensitivity coefficient value which was extracted as an average from mean voltage data of more than twenty probes operated over a large range of Mach and Reynolds numbers.

5.1 CALIBRATION CHARACTERISTICS OF SINGLE ELEMENT PROBES

Individual bridge voltage values of the single element hot wire probes were assembled in the form of a calibration plot showing bridge voltage versus mass–flux, each normalized to its reference value for an arbitrarily chosen test condition of $M = 0.4$, $P_T = 1$ ATMS, and $T_T = 72°F$. An example of such a plot is shown in Fig. 21.

These characteristics matched other results obtained from calibrations of similar probes in a research test and led to the definition of a single, average, sensitivity coefficient for mass–flux[3]:

$$S_{\rho U} = \frac{\partial\{\log(E/E_{ref})\}}{\partial\{\log(\rho U/(\rho U)_{ref})\}} = 0.15$$

This definition became the basis for conversion of the fluctuating parts of bridge voltages from single element hot wire probes to turbulence levels:

$$\frac{\sqrt{(\rho' u')^2}}{\overline{\rho U}} = \frac{1}{S_{\rho U}} \frac{\sqrt{e'^2}}{\bar{E}}$$

for single element probes

5.2 CALIBRATION CHARACTERISTICS OF X-WIRE PROBES

All cross wire probes contained geometrically identical sensor elements placed at 90° to each other. The fluctuating parts of the two elements were first brought to a common reference mean–voltage by applying a simple linear correction method, and then the difference and

the sum of the fluctuating parts of the signals were interpreted as lateral and stream–wise turbulence levels. Sensitivity coefficients for these types of probes were verified in a separate research test to be the same as those for a single element probe.

$$\frac{\sqrt{(\rho' v')^2}}{\overline{\rho U}} = \frac{\frac{1}{2}\sqrt{\left(e'_a - \frac{\bar{E}_a}{\bar{E}_b} e'_b\right)^2}}{S_{\rho U} \times \bar{E}_a}$$

$$\frac{\sqrt{\left(\rho' u'_{xv}\right)^2}}{\overline{\rho U}} = \frac{\frac{1}{2}\sqrt{\left(e'_a + \frac{\bar{E}_a}{\bar{E}_b} e'_b\right)^2}}{S_{\rho U} \times \bar{E}_a}$$

for cross–wire probes

The value of lateral component sensitivity was also verified with data from present tests by tracking the variation of the difference between mean voltages as a function of probe incidence angle while the probe–rake was pitched to ±2° during 5-hole cone probe calibrations. Governing equations relating the mean voltages and the mass–flux variable for the two wires of the X-wire probe were derived as:

$$E_{a;b} = E_{a;b,\alpha=0} \left\{ \frac{\rho U \mathrm{Sin}(45° \pm \alpha)}{\rho U \mathrm{Sin}(45°)} \right\}^{S_{\rho U}}$$

with α = probe angle to flow
for X-wire probe elements 'a' and 'b',
$+\alpha$ for 'a' and $-\alpha$ for 'b'

The difference between mean voltages for small probe angles was then deduced as a simple function of flow angle by applying small perturbation analysis principles:

$$\frac{1}{2}\left(\frac{E_a}{E_{a,\alpha=0}} - \frac{E_b}{E_{b,\alpha=0}} \right) = S_{\rho U} \times \alpha$$

for small α

Data for Mach numbers of 0.4 and 0.8, with the two X-wire elements operated at the same overheat ratio (ratio of the sensor resistance at operating conditions to that at standard reference temperature of 20°C), confirmed the value of sensitivity coefficient as 0.15, Fig. 22.

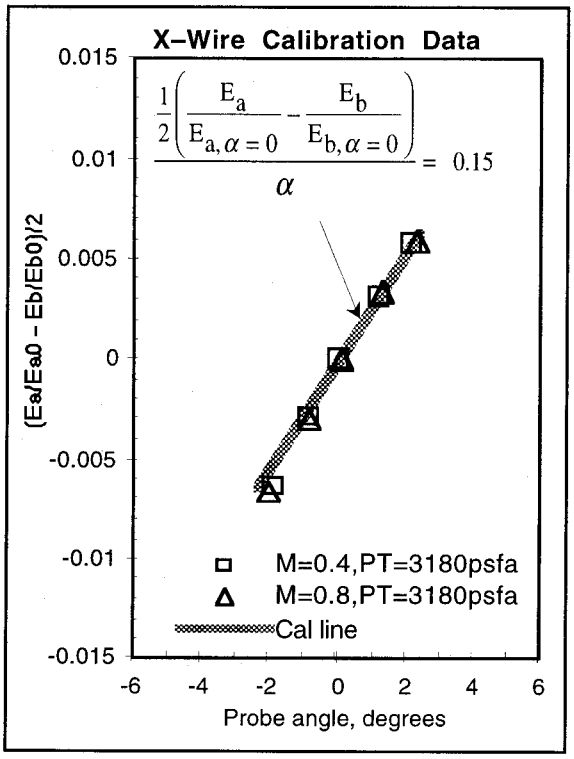

FIG. 22 X–WIRE PROBE CALIBRATION

It may be noted that lateral turbulence values were subject to a higher level of uncertainty because of the extra processing steps, but generally matched the streamwise turbulence values and will not be discussed further.

5.3 TURBULENCE LEVELS

Overall turbulence levels for a wide bandwidth of 1 Hz to 16 KHz were compared with levels measured in the tunnel before modernization in the absence of the flow conditioning system[5], Fig. 23.

The configuration listed as "Slots Normal" as noted earlier in this paper refers to the standard testing configuration for which all of the wall–slots remain open to provide blockage relief to the flow over the test article in the test section. Part of the wall flow escapes to the plenum chamber, driven by the blockage induced excess pressure at the wall and further aided by the suction induced by the diffuser flaps at the exit of the test section. Gap settings at the diffuser flaps can be adjusted to alter the relief flow. One other consequence of the "Slots Normal" configuration is the flow disturbances generated at the edges of the slots. These disturbances propagate to the core flow region of the test section and elevate the turbulence level as well as acoustics.

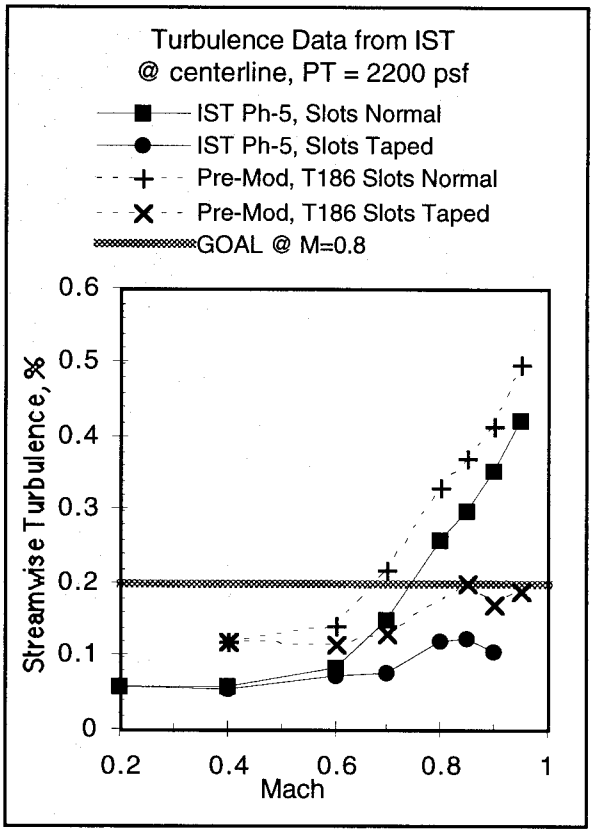

FIG. 23 TURBULENCE IN MODERNIZED TUNNEL COMPARED WITH PRE-MOD LEVELS.

It is anticipated that a clever treatment, yet to be devised, for the slot geometry and the slot fillers could significantly abate the elevated turbulence and acoustic levels caused by the edges of the slots. A measure of the potential gains from such treatment can be gleaned from the "Slots Taped" configuration in which every slot is fully blocked by adhesive tape running along the entire length of the slot and firmly adhering to slat surfaces flanking the slot. The reduction in turbulence level from "Slots Normal" to "Slots Taped" configurations is the potential flow quality gain that can be accomplished with acoustic treatment of every slot and its filler.

One feature that was not addressed in the modernization project because of funding limitations was the flow quality gain that accompanies slot treatment. Another related feature, to be discussed later in this paper, is the acoustics contribution emitted by the blades of the tunnel drive with a characteristic frequency that follows the rotational speed of the drive. This contribution may be suppressed by adding acoustic treatment somewhere in the tunnel leg between the drive and the test section, for instance in the turning vanes.

The acoustic contributions from slot noise and drive tones must be considered when the measured flow quality level is compared to the goals envisioned for flow quality in the modernization effort. Although the goal of 0.2% or better in turbulence at M = 0.8 was narrowly missed, the potential gain from slot treatment represented by the "Slots Taped" configuration clearly exceeds the goal by a good margin, Fig. 23. An even bigger margin can be shown in the spectral content, to be discussed later in this paper, when drive tone suppression treatment is added to the tunnel circuit to reduce its input to the test section flow disturbance environment.

Gains attributed to the TRS are evident from the drop in turbulence levels compared to data collected in the Pre–Mod flow quality test T186, Fig. 23. However, the turbulence reduction ratio, which characterizes the basic success of the TRS, cannot be directly read from the test section turbulence levels because the contributions from slot noise and drive tones do not even pass through the TRS. Ratios read from the present and pre–mod data pertaining to relatively low Mach numbers, say $M \leq 0.6$, provide a reasonable measure of the turbulence reduction ratio, in this case a ratio slightly larger than 2:1 which is consistent with expectations. Future measurements in the region of the TRS ahead of contraction will help refine this ratio and properly quantify the performance of the TRS.

5.4 STRUCTURE OF TURBULENCE

Spectra of turbulence signals offer a more detailed look into the various components that constitute the total turbulence level and thus help identify the relative importance of the different sources of flow perturbations in the tunnel. To accomplish the latter, it is desirable to catalog all possible sources of flow dynamics in the tunnel and associate each of those with a predicted primary frequency. Major sources in the 11-Ft TWT are the compressor, test section wall slots, test section exit diffuser, turning vanes, back–leg wide angle diffuser and heat exchanger.

Over the tunnel Mach range of 0.2 to 1.5, the compressor is operated in the range of 200 RPM to 720 RPM. This range of rotational speeds, in association with the blade counts in the different stages of the compressor, produce primary frequencies in the range of 180 Hz to 650 Hz.

Test Section wall slots are roughly 0.6 inch wide and 5 inch deep and may be expected to generate slot noise which contributes to the turbulence in the frequency range of 2.5 KHz to 3.0 KHz.

The exit diffuser stretches from the exit of the test section to the first set of turning vanes, a distance of about 150 feet, and may cause acoustic resonance frequencies around 7 Hz.

Turning vanes located at the four corners have flat plates contoured and precisely aligned to turn the flow smoothly and therefore exert only a small influence on flow quality, less than the disturbances from all other sources of flow dynamics. Among all the vane sets, set #4 just ahead of the contraction and the TRS is likely to have the largest effect, with secondary flow patterns from the curved passages and turbulence wakes of the vane trailing edges feeding into the TRS elements at frequencies in the range 5 Hz to 100 Hz.

The back–leg wide angle diffuser has a large wall angle of 30° which causes large scale unsteady flow separation zones with a periodicity exceeding several seconds. The heat exchanger installation, with its thick beams and girders which leave wide wake–flow trails and the heat exchanger panels, with their tubes and fins which introduce small scale turbulence, may be expected to add frequencies in the range 5 Hz to 200 Hz and perhaps even higher.

The above catalog of frequency attributes for the various disturbance sources in the tunnel makes it possible to take a closer look at the frequency spectra of test section turbulence and learn more about the hierarchy of those sources in the flow quality domain. The hierarchy, viewed in the flow quality arena, is not unique to the source, but is a function of one other variable, namely the Mach number which reflects the effects of compressibility in the flow. The role of Mach number is readily seen in a comparison between 1/3 Octave spectra for the "Slots Normal" configuration at M = 0.4 and M = 0.8, Fig, 24.

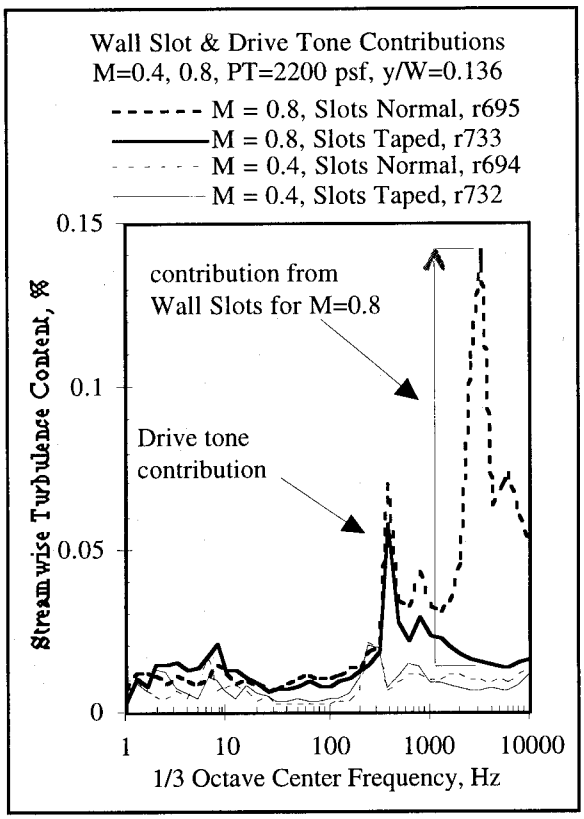

FIG. 24 TURBULENCE CONTRIBUTORS AND EFFECTS OF MACH NUMBER

Spectral content for M = 0.4 contains fairly short peaks at frequencies supplied by the test section exit diffuser and the tunnel drive. These peaks are sharper and taller for M = 0.8, and are combined with yet another, much taller, peak at frequencies supplied by the wall slots in the test section. Elevated amplitudes of these peaks are direct measures of the nature, growth, and propagation of flow disturbances when compressibility effects begin to play a role in the flow–field.

Spectral plots of the turbulence signals also offer clear indications of changes in the contributions of any given source when suppression treatment is implemented to mitigate the influence of that source. "Slots Taped" represents one such treatment by which the slot noise is entirely eliminated, and a reduction of more than 10:1 is evident in the content at frequencies (2.5 Khz to 3.0 KHz) associated with the slot for M = 0.8, Fig. 24. For the case of M = 0.4, the contribution from slots is small and, as expected, so is the reduction in the spectral amplitudes at the slot noise frequency.

Comparisons of the spectral content between current and Pre–Mod turbulence signatures make

it possible to focus on just the turbulence content passing through the flow conditioning systems, avoiding the content pertaining to other propagation paths in the rest of the tunnel, and thus getting a better measure of the gains accomplished by the flow conditioning systems, Fig. 25.

Slot noise is generated by the test section walls, and neither the TRS nor the back–leg flow smoothing system, has any role in the impact of slot noise. Tones generated by the compressor predominantly travel upstream along the cross leg and the test section exit diffuser to inundate the test section flow, and again, neither the TRS nor the back-leg system has any role to play. Once these components of the spectra are removed and a turbulence reduction ratio is constructed by marching along the spectra to calculate the ratio of turbulence content from Pre–Mod to current status, the ratio varies from 2:1 to 4:1, Fig. 25. This is a truer indication of the gains from the flow systems than the ratio of 2:1 suggested earlier by the total turbulence levels.

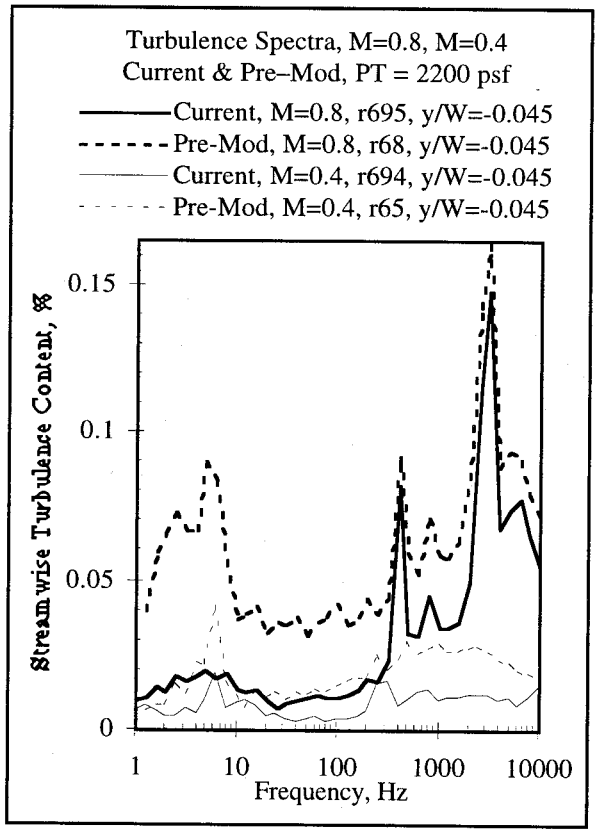

FIG. 25 TURBULENCE REDUCTION AS A FUNCTION OF CONTRIBUTORS

6. PRESSURE DROP FROM TRS

Pressure drop characteristics of the TRS elements, honeycomb and screens, were measured with pitot–static probes positioned at different stations in the region of the TRS, Fig. 26. Data matched expectations based on simulation test results[5] and existing literature.

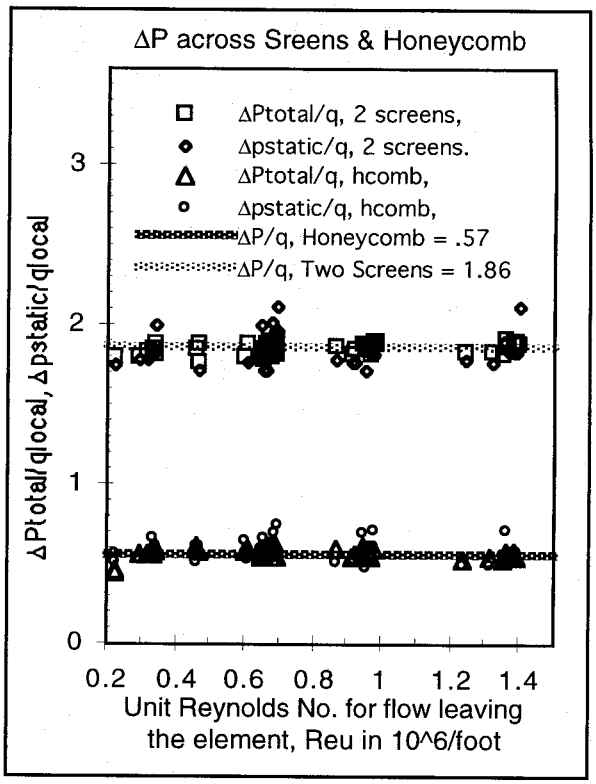

FIG. 26 PRESSURE DROP CHARACTERISTICS OF HONEYCOMB AND SCREENS.

7. ACOUSTIC DATA

Acoustic probes, the ten degree cones with two pressure transducer installations, were tested for response characteristics by placing the probes in front of an electrically excited speaker, running the speaker to various sound levels and frequency contents, and checking the output of the transducers against an adjacent transducer. This step was used only to verify the response characteristics of the mounted transducers as installed on the cone probes, not for calibration which was accomplished in a much more controlled setting with selected inputs to the reference port of the transducers.

Acoustics in the test section are the result of contributions arriving from many sources in the tunnel. Although no form of acoustic suppression was introduced in the current modernization effort,

it may be expected that the flow conditioning systems might bring some improvement in the acoustic levels in the test section. Such improvement may be masked in the acoustic measurements because of the change to composite compressor blades during the modernization effort. Current results pertain to composite blades in the tunnel compressor whereas the Pre–Mod data[6] correspond to aluminum blades. Any reduction in acoustics will be a combined effect of the composite blade characteristics and the flow conditioning systems.

7.1 ACOUSTICS LEVELS

Comparisons of fluctuating pressure coefficient data between current and Pre–Mod tests suggest that there may have been some reduction in the acoustic level, Fig. 27. Reduced acoustics from "Slots Normal " to "Slots Taped" is attributed to the disturbances generated at the edges of the slots, discussed earlier in the context of turbulence levels. As with turbulence levels, the potential for reducing the acoustics by some form of treatment of the slot geometry and the slot fillers is significant. The potential gain from improved slot fillers alone can be impressive as demonstrated by Steinle[7] in exploratory trials at NASA Ames 14-Ft TWT.

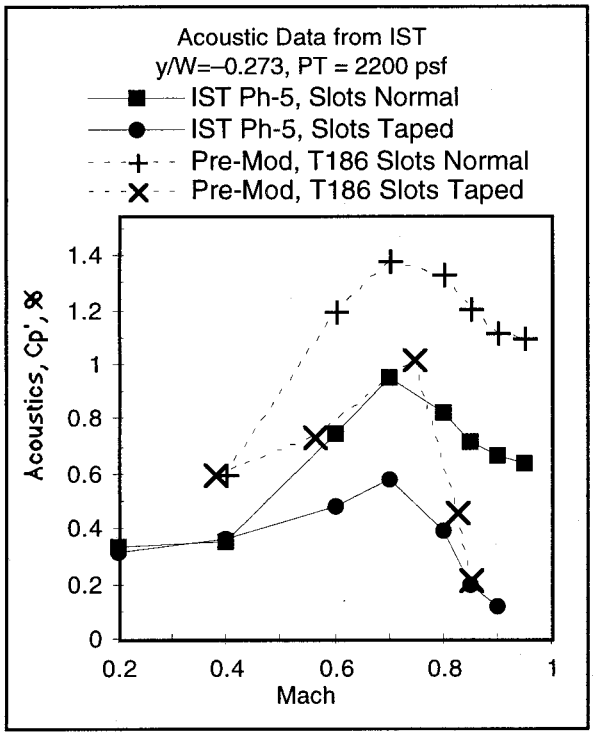

FIG. 27 ACOUSTICS IN MODERNIZED TUNNEL COMPARED WITH PRE-MOD LEVELS.

The drop in acoustic levels at higher Mach numbers, above M ≈ 0.7, may be attributed to reduced transmission from one of the contributors, the compressor tones. At lower Mach numbers, the flow speeds in the transition diffuser are low enough for the acoustics from the compressor to propagate at full strength against flow, into the test section without much attenuation. At higher Mach numbers, flow in the transition diffuser approaches sonic conditions and begins to block the propagation of drive tones, thus causing the trend of diminishing acoustic levels at Mach numbers above M = 0.7.

7.2 STRUCTURE OF ACOUSTICS

Relative impacts of individual contributors to the overall acoustic levels can be readily seen in the spectra of the signals from the cone probe transducers. The variety of sources that cause disturbances in the tunnel circuit and the frequencies associated with those were discussed in an earlier chapter of this paper in the context of turbulence. Of interest to the acoustics are two contributors: the compressor tones and the test section wall slot generated noise, Fig. 28.

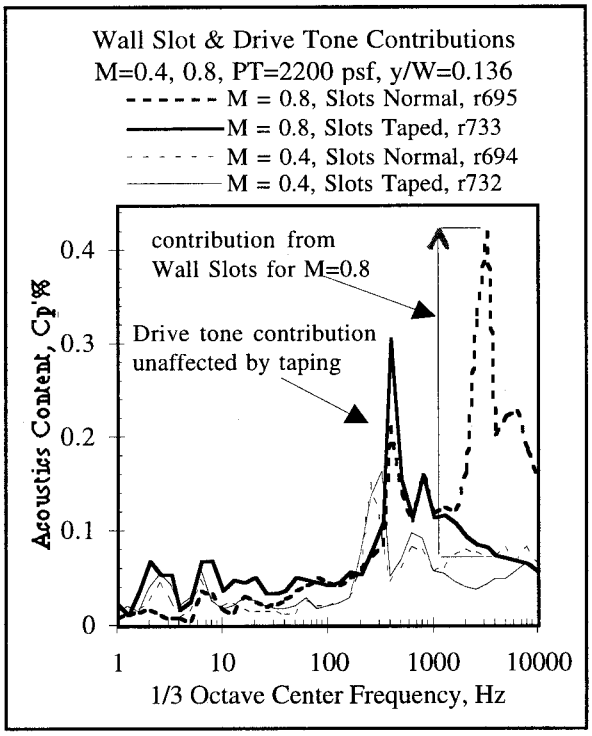

FIG. 28 ACOUSTICS CONTRIBUTORS AND EFFECTS OF MACH NUMBER

Acoustics from the compressor predominantly migrate upstream via the test section exit diffuser, against the high velocity flow in the transition diffuser and inundate the test section to produce high acoustic levels. This contribution becomes much higher with increase of Mach number, as evidenced in the comparison of spectra between M = 0.4 and M = 0.8, Fig. 28. Not shown here is the trend that accompanies further increases in Mach number, for which the flow speed in the transition diffuser approaches sonic conditions, prevents upstream travel of acoustics, and so causes a drop in the test section acoustic content in the drive–tone related frequency range.

The other contribution of interest is the test section wall slot generated noise in the frequency range of 2 to 4 KHz. As with turbulence, the "Slots–Taped" configuration clearly identifies the contribution from the slots which elevates the acoustics in the test section, Fig. 28. Much may be gained in terms of acoustic suppression by adding acoustic treatment to the slots.

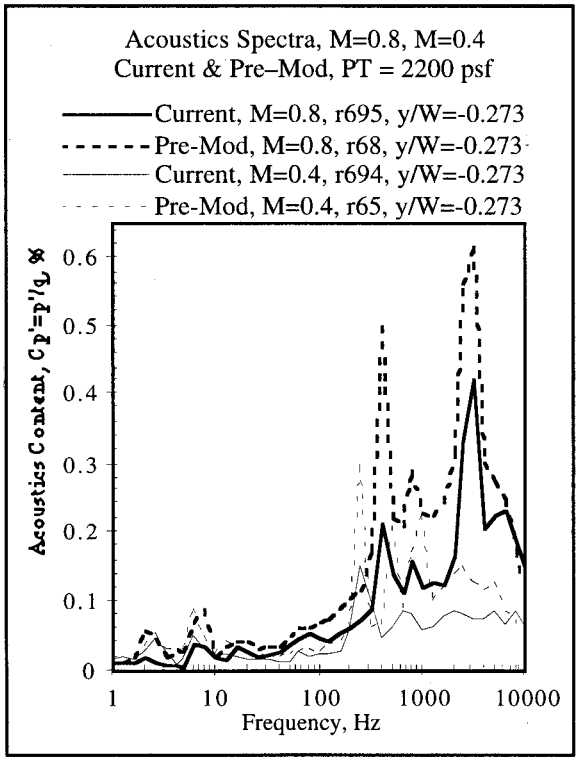

FIG. 29 ACOUSTICS AFTER MODERNIZATION AS A FUNCTION OF CONTRIBUTORS

Changes in test section acoustics brought by upgrades introduced in the modernization project may be quantified in greater detail by a comparison of the spectra in measurements made before and after modernization, Fig. 29. Reductions appear obvious, but the cause for this reduction is less clear. Perhaps it is best explained as the cumulative effects of flow quality enhancement systems and compressor blade replacement.

8. CONCLUDING REMARKS

The modernization project, begun in 1989 and completed in 1998, brought many upgrades to the NASA Ames 11-by 11-Foot Transonic Wind Tunnel. Included among those upgrades were a turbulence reduction system with a honeycomb and two screens, a flow smoothing system in the back leg tandem diffuser, an improved drive motor control system, and a full replacement set of composite blades for the compressor.

A flow quality baseline for the tunnel in its configuration before modernization was available from measurements performed with an instrumented 8-foot span rake traversed vertically in the test section. The same rake was used after modernization in late 1999 as a part of the Integrated System Tests (IST), to obtain data on flow quality of the upgraded tunnel. Because of the focus of the IST activities, the flow quality surveys as well as the extent of instrumentation were somewhat limited, relegating the bulk of flow quality mapping to Calibration Tests which will follow. The primary objective of these IST flow quality tests was to document the nature of flow quality in the tunnel now and to provide a preliminary assessment of the effectiveness of the tunnel upgrades.

The measurements clearly revealed substantial improvements in flow angularity and significant reductions in turbulence level for both full–span and semi–span testing configurations, thus making the flow quality of the tunnel one of the best among existing transonic facilities. Overall flow quality levels for the current configuration of the tunnel are listed in contrast to the Pre-Mod levels in the following Table:

TEST SEC. IN NORMAL CONFIG. CORE REGION (8-FT) PT = 2200 PSF	PRE-MOD	CURRENT
UPFLOW Angularity, deg, M=0.8	-.06° ± .1°	- .06° ± .08°
CROSSFLOW Ang., deg, M=0.8	.13° ± .2°	.07° ± .08°
Turbulence, %, M=0.4	.12	.06
Turbulence, %, M=0.8	.32	.25
Acoustics, Cp', %, M=0.4	.6	.36
Acoustics, Cp', %, M=0.8	1.3	.8

Some of the numbers may not provide a complete measure of the gains brought by the tunnel upgrades. Spectral decomposition of those numbers will be required, as illustrated in earlier chapters of this paper, before the gains may be correctly quantified. Measurements during the IST tests spanned a range of tunnel pressures, Mach numbers and test section wall slot configurations. Data presented in this paper are only a sample of the entire database, much of which is still undergoing detailed analysis. However, the data in this paper are typical of other test conditions and deliver the message about the substantial improvements accomplished with the modernization effort. Further upgrades including drive-tone acoustic suppression, test section wall slot treatments and augmented plenum suction mode can bring additional gains in the flow quality of the tunnel, especially with regard to acoustics, and its contribution to the turbulence.

9. NOMENCLATURE AND ABBREVIATIONS

NOMENCLATURE:

a = speed of sound, = $\sqrt{\gamma RT}$

Alpha = 5-Hole Probe Pitch Angle setting in the tunnel coordinate system
(= probe pitch angle for ø=0°)
(= negative of probe pitch angle for ø=180°)
(= probe yaw angle for ø=90°)

Beta = 5-Hole Probe Yaw Angle setting in the tunnel coordinate system
(= probe yaw angle for ø=0°)
(= negative of probe yaw angle for ø=180°)
(= probe pitch angle for ø=90°)

C'_p = Fluctuating Pressure Coefficient
= $\sqrt{\overline{p'^2}}/q_{\text{Test Section}}$ (acoustic coefficient)

CK0 = 5-Hole Probe Calibration Coeff. (see chapter 4)

CK1 = 5-Hole Probe Calibration Coeff. (see chapter 4)

CPTC = Yaw Pressure Coeff. (see chapter 4)

CPTU = Pitch Pressure Coeff. (see chapter 4)

D = Diameter of settling chamber, = 39 ft.

E = Anemometer Bridge Voltage for sensor in flow

H = Height of the Test Section, = 11 ft.

KPHI = 5-Hole Probe rotation factor (see chapter 4)

K0 = 5-Hole Probe Calibration Coeff. (see chapter 4)

K1 = 5-Hole Probe Calibration Coeff. (see chapter 4)

m = mass flux = ρU

M, M_{TS} = Test Section Mach number

M_{avg} = Average Mach number for the cross section, calculated from stream–tube area relations with test section conditions

P_T = Total Pressure in Test Section

p' = fluctuating (ac) component of pressure

p'_{rms} = root mean square of pressure fluctuations,

$$= \sqrt{\overline{p'^2}} = \sqrt{\lim_{t\to\infty}\left\{\frac{1}{t}\int_{t=0}^{t} p'^2\, dt\right\}}$$

P1, P2: Pitch sensing taps on the 5-hole probe

P3, P4: Yaw sensing taps on the 5-hole probe

P5: Total pressure tap on the 5-hole probe

P6: Static pressure tap on the 5-hole probe

q = Dynamic Pressure = $\frac{1}{2}\gamma pM^2$

Re_u = Unit Reynolds number = $\rho U/\mu$, /ft

R_G = Perfect Gas Constant for air
= 1716 $ft^2/sec^2\,°R$

T = temperature (absolute)

T_T = Total Temperature in Test Section.

U = Flow Velocity

U_{avg} =Average Flow Velocity calculated from stream–tube area relations:

$$U_{avg} = M_{avg} \times \sqrt{\frac{\gamma \times R_G \times T_T}{1+\frac{(\gamma-1)}{2}M_{avg}^2}}$$

UK0 = 5-Hole Probe Calibration Coeff. (see chapter 4)

UK1 = 5-Hole Probe Calibration Coeff. (see chapter 4)

U_∞ = freestream velocity (mean)

u', v', w' = fluctuating parts of flow velocity

uxv', uxw' = u' derived from cross wire probes

U = mean part of flow velocity, u(t) = U + u

W = Width of the Test Section, = 11 ft.

x, y, z = streamwise, spanwise & vertical coordinates, zero at centerline of the flow passage, z is positive for top, y is positive for south.

γ = ratio of specific heats for air, = 1.4

μ = viscosity of the flow medium, =

$$2.270\frac{T^{1.5}}{T+198.6}10^{-8}, \frac{\text{lb sec}}{\text{ft}^2}, \text{ for air at T°R}$$

ø = 5-Hole Probe rotation (roll) angle, degree

$(\rho u)'$ = fluctuating part of streamwise mass flux = m'

$$\text{Streamwise Turbulence} = \frac{\sqrt{\overline{(\rho' u')^2}}}{\overline{\rho U}}$$

$(\rho v)'$ = fluctuating part of spanwise mass flux

$(\rho w)'$ = fluctuating part of vertical mass flux

ABBREVIATIONS:

ADF= Annular Diffuser Flaps on the nacelle in the back–leg.

ATV = Annular Turning Vanes at the entry to the Wide Angle Diffuser in the back-leg.

TRS = Turbulence Reduction System ahead of contraction in the settling chamber.

TWT = Transonic Wind Tunnel

10. REFERENCES

1 Belter, Dale L., "Comparison of Wind Tunnel Data Repeatability with Uncertainty Analysis Estimates," AIAA–98-2714, 20th AIAA Advanced Measurement and Ground Testing Technology Conference, Albuquerque, NM, June 15-18, 1998

2 Kmak, F.J., "Modernization and Activation of the NASA Ames 11-by 11-Foot Transonic Wind Tunnel," Paper# 2000–2680, 21st AIAA Advanced Measurement and Ground Testing Technology Conference, Denver, CO, June 19-22, 2000.

3 Murthy, S. V., Kmak, F. J., Boone, A. R., and Muzzio, D. E., "Test Data Summary Report on Simulation Tests in BLASTANE for Design and Validation of TRS for 11-FT TWT," # 327–8910–XT1020, Unitary Mod. Project, NASA Ames Res. Center, Moffett Field, CA, Dec. 1995.

4 Murthy, S. V., Kmak, F. J., Boone, A. R., and Muzzio, D. E., "Test Data Summary Report on Simulation Tests in BLASTANE for Design and Validation of Flow Conditioning Systems for Annular and Wide Angle Diffusers in NASA Ames 11-FT TWT," # 327–8910–XT1016, Unitary Mod. Project, NASA Ames Res. Center, Moffett Field, CA, Apr. 1995.

5 Murthy, S. V., Kmak, F. J., and Koss, B. R., "The Design and installation of Turbulence Reduction System for the NASA Ames 11-by 11-Foot Transonic Wind Tunnel," Paper# 98–2705, 20th AIAA Advanced Measurement and Ground Testing Technology Conference, Albuquerque, NM, June 15-18, 1998.

6 Richey, Scott, "Results of 11-Ft Transonic Wind Tunnel Turbulence Test– Final Report, Test# 186-1-11," submitted to UPWT Modernization Project, NASA Ames Research Center, Moffett Field, CA, Dec. 9, 1994.

7 Steinle, Frank W., "Development of the Porous-Slot Geometry of the NWTC Test Section," Paper# 97-0097, 35th Aerospace Sciences Meeting and Exhibit, Reno, NV, Jan. 6-10, 1997.